Letter

Full Energy Range Resonant Inelastic X-ray Scattering of O_2 and CO_2: Direct Comparison with Oxygen Redox State in Batteries

Zengqing Zhuo, Yi-sheng Liu, Jinghua Guo, Yi-de Chuang, Feng Pan,* and Wanli Yang*

Cite This: *J. Phys. Chem. Lett.* 2020, 11, 2618−2623

Read Online

ACCESS | Metrics & More | Article Recommendations | SI Supporting Information

ABSTRACT: The evolving oxygen state plays key roles in the performance and stability of high-energy batteries involving oxygen redox reactions. Here, high-efficiency full energy range O-K mapping of resonant inelastic X-ray scattering (mRIXS) was collected from O_2 (O^0) and CO_2 (O^{2-} with strong covalency) molecules and compared directly with Li_2O_2 (O^-) and the oxidized oxygen state in representative Na/Li-ion battery electrodes. Our results confirm again that the critical mRIXS feature around the 523.7 eV emission energy is from intrinsically oxidized oxygen, but not from the highly covalent oxygen state (CO_2). The comparison of the mRIXS profile of the four different oxygen states, i.e., O^{2-}, O^-, O^{n-} ($0 < n < 2$), and O^0, reveals that oxygen redox states in batteries have distinct widths and positions along the excitation energy compared with Li_2O_2 and O_2. The nature of the oxidized oxygen state in oxide electrodes is thus beyond a simple molecular configuration of either peroxide or O_2.
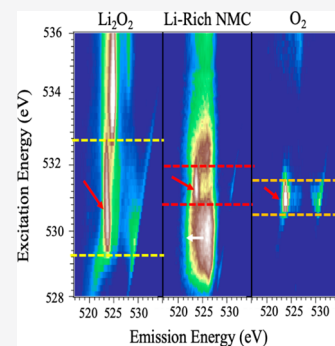
The chemical state of oxygen in various electrochemical systems has recently attracted much attention because it holds the promise of performance improvements; however, it is also believed to be responsible for detrimental effects on stability and sluggish kinetics.[1,2] A fervent debate on how to understand and control the unconventional oxygen states have triggered intensive studies in both alkali-ion batteries and catalytic systems.[1,3,4] Nondivalent model oxygen systems, O_2,[5] and peroxo-species[6] have been proposed to explain the oxidized oxygen state in battery materials. However, the extremely strong transition-metal dependence of the oxygen redox activities in battery electrodes indicates that molecular oxygen systems may not necessarily be the fundamental model of the oxidized oxygen state in these electrochemical systems.

Experiments often find oxygen activities in different forms with unclear connections,[7,8] which mainly involve (i) the O_2 release and associated surface reactions,[9] and (ii) the intriguing species of lattice oxidized oxygen.[2] However, oxygen in an oxide electrode is always involved in battery operations through the strong hybridization with the transition metals,[10] with or without oxygen redox activities.[11] It is therefore equally important to test a highly covalent O^{2-} model system, such as CO_2, to clarify the differentiation between the intrinsically oxidized oxygen state and the modified oxygen state through covalency. Therefore, a direct comparison through a reliable probe of the four different oxygen oxidation states, i.e., O^0(O_2), O^-(Li_2O_2), highly covalent O^{2-}(CO_2), and more importantly, the O^{n-} ($0 < n < 2$) species in battery electrodes, is of both fundamental and practical importance for understanding the chemical reactions involved in a wide range of energy applications including alkali-ion, Li−air batteries, and catalytic systems.[1−4]

Several spectroscopic studies of O_2 and CO_2 were reported on the basis of O K-edge X-ray absorption spectroscopy (XAS) and resonant inelastic X-ray scattering (RIXS) at particular excitation energies.[12−15] Especially, RIXS studies of O_2 molecules at characteristic excitation energies have resolved the fine structure of vibronic modes of O_2 with the focus on the low-energy excitations close to the elastic peaks.[13] RIXS studies of CO_2 have shown that the molecule is a good model system to study the symmetry breaking effect on the intermediated excited states during RIXS process.[14,15] While these previous studies revealed interesting results with focused discussions on the vibrational coupling, our recent studies in battery materials involving oxygen redox activities show that the oxidized oxygen displays two characteristic features in mapping of RIXS (mRIXS); one is an enhanced low-energy excitation feature close to elastic peaks,[5,16] and the other is a prominent feature at ∼523.7 eV emission energy.[8,11,16−20] More importantly, analysis strongly suggests that a full mRIXS profile across a wide energy range of both excitation and emission energies is critical for studying nondivalent oxygen states due to three aspects:[17,18,21] (i) Only a full mRIXS profile of the nondivalent oxygen state along both excitation and emission energies could reveal the spectroscopic contrasts in different species. For example, mRIXS of Li_2O_2 displays a much broadened mRIXS feature along the excitation energy
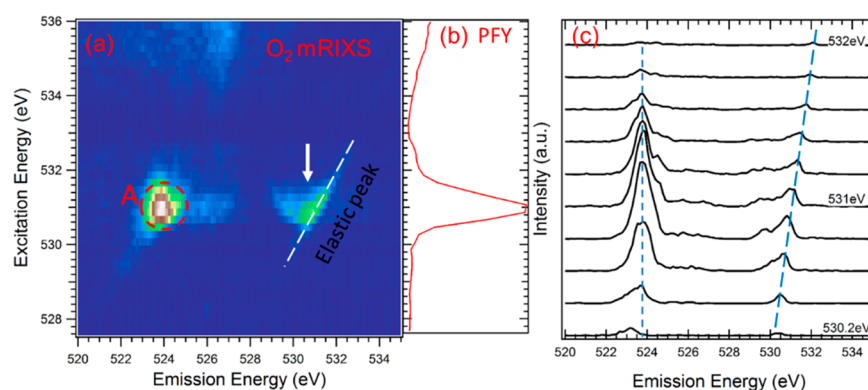
Figure 1. (a) O K-edge mRIXS of O_2. The map is dominated by two characteristic features, A, centered at 523.7 eV emission energy (red circle) and low-energy excitations close to elastic line (white arrow). (b) O-K PFY of O_2, which is obtained by the integration of the mRIXS signals at each excitation energy. (c) Individual O K-edge RIXS cuts of O_2 with excitation energy range of 530.2−532 and 0.2 eV step.

compared with that of battery electrodes, while the individual RIXS spectra at ∼531 eV excitation energy display similar features of oxidized oxygen.[21] (ii) Critical features of oxidized oxygen may appear at excitation energies completely off the absorption peaks, which could only be detected in mRIXS with a fine experimental step along excitation energies.[18] (iii) The full profile revealed by energy-range mRIXS could enable quantitative studies of the nondivalent oxygen states in some system,[17] but a reliable quantification is only feasible through the integration of the total intensity along both the excitation and emission energy axes accessible through a mapping of RIXS (mRIXS). Therefore, it is crucial to perform the full energy range mRIXS experiments of O_2 and CO_2, which remains missing the field, and compare them directly with other oxygen systems to reach a complete and direct comparison.

In this work, we first report the full energy range mRIXS results of O_2 and CO_2 gas molecules through the established high-efficiency RIXS and soft X-ray gas cell systems.[22,23] We then compare the full mRIXS profiles of O^0 (O_2), O^- (Li_2O_2), O^{2-} (CO_2, highly covalent), and the O^{n-} ($0 < n < 2$) state in representative Na-ion and Li-ion battery systems.[17,20,21] Although CO_2 is a highly covalent system with an ill-defined O^{2-} valence, the data show that the covalency effect is different from that for all other intrinsically oxidized oxygens, which always display a characteristic mRIXS feature at 523.7 eV emission energy with a varying excitation energy around 531 eV. Our direct comparison between the three different oxidized oxygen systems reveals distinct mRIXS profiles between them. This is the first time a full profile of O_2 and CO_2 mRIXS is reported and different nondivalent oxygen states are compared with each other directly. The direct comparison suggests that the oxidized oxygen state in the battery electrode is not simply a molecular configuration as in either peroxides or O_2 gas.

O K-edge mRIXS measurements were performed in the high-efficiency iRIXS endstation at Beamline 8.0.1 of the Advanced Light Source at Lawrence Berkeley National Laboratory.[22] mRIXS data were collected through a high-transmission soft X-ray spectrometer with energy resolution of about 0.3 eV on emission energy.[24] A series of RIXS spectra have been recorded across the O K-edge with steps of 0.2 eV in excited energies. The recorded spectra were then plotted in color scale and combined into a mRIXS map.[22] The partial fluorescence yield (PFY) sXAS data were extracted from the

mRIXS results by integrating the intensity at each excitation energy.[18] All the data have been normalized to the beam flux measured by a clean gold mesh upstream of the endstation. The mRIXS maps shown in this work are accomplished within 15 min. Experimental details of Li_2O_2,[21] charged NMMO ($Na_{2/3}Mg_{1/3}Mn_{2/3}O_2$),[17] and charged Li-rich NMC ($Li_{1.17}Ni_{0.21}Co_{0.08}Mn_{0.54}O_2$),[20] were previously reported. Note we compare the mRIXS results with only fully charged electrodes where oxidized oxygen, i.e., O^{n-} ($0 < n < 2$) has been confirmed.[17,20] All solid-state samples were handled with zero air exposure, and data were collected with low X-ray flux with itinerary sample throughout the experiment to eliminate radiation damage issues.[25] For measuring the O_2 and CO_2 gas phase samples, the photon beam entered and exited a homemade gas cell filled with gas through a 100 nm thick silicon nitride window.[23] For a direct comparison, all energy values reported here are calibrated in the same way by measuring TiO_2 as a reference.

Figure 1a shows the experimental O K-edge mRIXS results of O_2 gas with the excitation energy (vertical axis) range 527.6−536 eV. The integration of the mRIXS intensity along emission energies (horizontal) provides the partial fluorescence yield (PFY) signal of XAS, which is shown in Figure 1b and consistent with previous reports.[12] Representative individual RIXS spectra excitation in the energy range 530.2−532 eV are shown in Figure 1c.

Technically, full-energy-range mRIXS records intensity distribution upon the energy of the fluorescence photons, i.e., the emission energy, at each excitation energy in the XAS scan range, thus forming a two-dimensional intensity plot as a function of both emission energy and excitation energy.[18] For the O_2 mRIXS, the whole map is dominated by a strong feature A centered at 523.7 eV emission energy and 531 eV excitation energy (Figure 1a), in addition to the low-energy loss features close to the elastic line (white dashed line). The RIXS spectra in Figure 1c further reveal the fine satellite structures of these two groups of features. It is clear that these features lead to the main O K-edge XAS peak (Figure 1b). According to the previous study,[12] this absorption feature around the 531 eV excitation energy corresponds to the transition between the 1s core electron to the initially half-filled π^* orbital. So the prominent feature A in mRIXS stems from the decay of electrons after the electron excitations from O 1s to the unoccupied π_g^* state. Therefore, the final state involved in the RIXS process that leads to feature A is equivalent to an excited
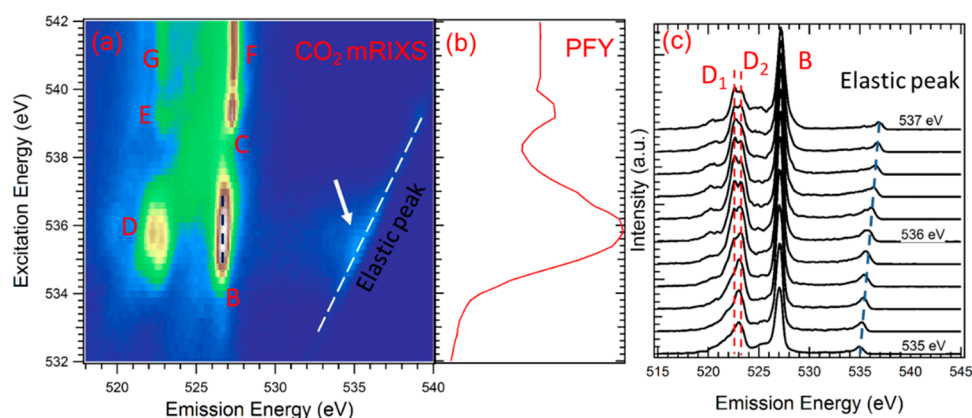
Figure 2. (a) O K-edge mRIXS of CO_2. Seven groups of features are observed, as indicated by the white arrow on the low-energy excitations and the letters of B−G. Group D consists of two features D_1 and D_2. (b) O K-edge PFY of CO_2, which is obtained by the integration of the mRIXS signals at each excitation energy. (c) Individual O K-edge RIXS cuts of CO_2 with an excitation energy range of 535−537 eV of 0.2 eV step. Features D_1 and D_2 are clearly resolved.

electron into the unoccupied O-2p molecular orbital. Because O^{2-} has only fully occupied 2p orbitals, this suggests again that the mRIXS feature with 523.7 eV emission energy is a fingerprint of the oxidized oxygen state, same as that for Li_2O_2.[21] However, it is a critical observation here that, although with the same emission energy of 523.7 eV, the overall profile of this oxidized oxygen feature along the excitation energy is dramatically different between Li_2O_2 and O_2, which will be elaborated on later in this work.

Other than feature A, two different types of features should also be noticed in Figure 1a,c. First, the weak signal shift below the excitation energy 530.6 eV is a Raman-like feature due to the strong excitation energy dependencies near the X-ray absorption edge.[26] Second, low-energy excitation features are observed at the same excitation energy of 531 eV, indicated by the white arrow in Figure 1a. These satellite features are observed at the 0−2 eV energy loss range close to the elastic line (white dashed line), related with nuclear vibrational excitations that were studied in detail before.[13] Note that an enhancement of such low-energy excitation features is also observed in battery electrodes with oxygen redox activities.[16]

Compared with O_2, CO_2 is a more complex system and could be considered as a linear molecular with full-filled HOMO in $D_{\infty h}$ symmetry. Parts a and b of Figure 2 display the O K-edge mRIXS and PFY results, respectively, of CO_2 gas with the excitation energy range 532−542 eV. The detailed RIXS line shapes with excitation energy range 535−537 eV are displayed in Figure 2c. Because CO_2 is a typical O^{2-} system, the RIXS intensity is observed only above ~534 eV excitation energies. This is expected because the low-energy excitation around 531 eV is characteristic of the oxidized oxygen, as discussed above for both O_2 and Li_2O_2.[21] However, it is important to note that CO_2 is a highly covalent system with an ill-defined O^{2-};[27] still, the 523.7 eV emission feature at around 531 eV excitation energy does not emerge in CO_2. Such an observation clearly shows that the specific mRIXS feature assigned to the oxidized oxygen states represents the intrinsic oxidized oxygen state that is different from a modified O^{2-} state from covalency or hybridization.

Overall, the mRIXS features of CO_2 consist of many groups, as marked on Figure 2a as features B−G. Additionally, low-energy excitations (white arrow) around excitation energy 536 eV could be seen, which is within 2 eV to the elastic peaks and

again due to nuclear vibrational excitations as in the case of O_2.[13] Some of the individual RIXS spectra around the excitation energies of 536 eV (B and D) and 539 eV (C and E) were discussed before with the focus on the symmetry breaking effect on the vibrational coupling.[14,15] Here, the wide energy range mRIXS results provide a clear overall contrast between all these features upon excitation and emission energies, as well as two new features (F and G) revealed at even higher excitation energies above 540.4 eV. Because the mRIXS patterns are much more complex than that of O_2, below we employ a molecular orbital schematic (Figure 3) to discuss the electronic origins and energy configurations in details.

The comparison between the mRIXS map (Figure 2a) and XAS-PFY (Figure 2b) shows that the features B/D and C/E corresponding to the 536 and 539.4 eV excitation peaks in XAS, which are known to be from the excitations from the 1s core electron to the π^* and σ^* orbital, respectively,[14,15] as schematically shown in the top two excitation channels in Figure 3. The emission energy of these four features varies but are roughly in two groups with relatively low (E and D) and high (B and C) energies, which originates from the different energy levels of the decaying valence electrons at the $1\pi_u$ and $1\pi_g$ states, as indicated by the different lengths of the red dashed lines in Figure 3. Note feature D consists of two features D_1 and D_2 at 522.3 and 522.8 eV emission energies, which could be seen clearly in the RIXS spectra in Figure 2c. This was the central topic in previous studies, which interpreted the splitting as the results of the symmetry breaking effect of the core hole states in CO_2.[14,15,28] While the features F and G have not been reported and analyzed before, they correspond to a much higher excitation energy and their overall profile displays fairly vertical lines with constant emission energies, which is a typical sign of the nonresonant valence electron decays when the core electrons are excited into high-energy states away from the absorption edge, i.e., the so-called nonresonant X-ray emission or fluorescence signals.[18] Although the features B (D) and C (E) are from the same decays of $1\pi_g$ ($1\pi_u$) electrons to the core hole, they display small differences in emission energies because the valence states are reconfigured differently with the different excitations, i.e., resonant effect in the "R"IXS process. But when the excitation energy becomes far above the
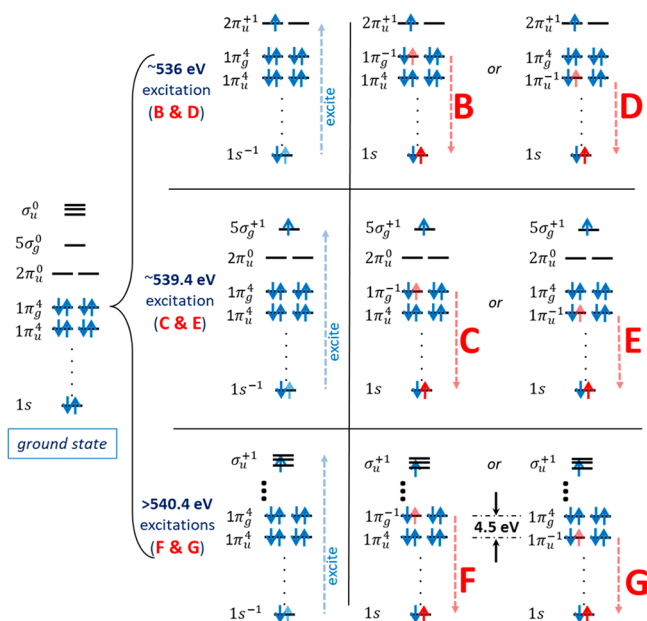
Figure 3. Schematic electronic configuration of CO_2 and the corresponding RIXS process based on single electron approximation. The CO_2 ground state is displayed on the left. Intermediate states defines the three groups of excitation energies of the mRIXS features. The electronic state is marked as, for example, $1\pi_g^{-1}2\pi_u^{+1}$, where -1 means electron hole present at the $1\pi_g$ orbital while $+1$ means extra electron present at the $2\pi_u$ orbital. Letters B−G indicate the decay processes that correspond to the 6 groups of mRIXS features shown in Figure 2a. F and G are nonresonant emission features that could be used to extract the 4.5 eV energy difference between the $1\pi_u$ and $1\pi_g$ molecular orbitals.

absorption edge, the emission signals get decoupled from the excitations and become nonresonant,[18] leading to the fixed emission energy at high excitation energies of features F and G. Therefore, the 4.5 eV difference in emission energies between the feature F and G is a direct probe of the energy difference between the $1\pi_u$ and $1\pi_g$ orbitals (Figure 3). In summary, the excitation energies of the mRIXS features of CO_2 are defined

by the electron excitations, while the emission energies are defined by the decays from different valence states.

With all the mRIXS features of O_2 and CO_2 interpreted, we could now compare directly the full mRIXS profile of the different oxygen states. As discussed in the introduction and the analysis of the two gas molecules above, only nondivalent oxygen states could display the ~531 eV low excitation energy feature, and the critical comparison is on the characteristic ~523.7 eV emission feature of the oxidized oxygen states, i.e., $O^0(O_2)$, O^- (Li_2O_2), and the O^{n-} ($0 < n < 2$) state in representative Na-ion and Li-ion battery systems.

Figure 4 displays the full mRIXS profile of Li_2O_2,[21] a fully charged $Na_{2/3}Mg_{1/3}Mn_{2/3}O_2$ (NMMO) electrode during the initial cycle,[17] a fully charged $Li_{1.17}Ni_{0.21}Co_{0.08}Mn_{0.54}O_2$ (Li-rich) electrode during the initial cycle,[20] and O_2. The choice of the two-electrode materials is based on the clear evidence of oxidized oxygen state in their charged states.[17,20] First, all these oxidized oxygen species display the characteristic mRIXS fingerprint ~523.7 eV emission energy (red arrows). However, the full mRIXS profile reveals different distributions of these oxidized oxygen features along excitation energies, with a color scale showing the same horizontal expansion along emission energy: Li_2O_2 displays the longest distribution and O_2 gas displays the shortest (Figure 4a). Detailed analysis of the feature width through quantitative peak fitting is provided in Figures S1−S3. Second, these oxidized oxygen features center at different excitation energies. This could be clearly seen from the sPFY (super Partial Fluorescence Yield[17]) spectra from the integration of the mRIXS intensity within a ±0.5 eV window to the characteristic 523.7 eV emission energy. The sPFY shoulders at 528−530.5 eV excitation energy are from the strong hybridization feature of the transition-metal (TM) 3d states, which is always heavily mixed with the oxidized oxygen feature.[10,18] We note that the profile contrast along the excitation energy could also be seen from the sPFY plot (Figure 4b), and this observation does not depend on the sPFY integration window size (0.2−1 eV).

Additionally, all systems display an enhanced low-energy excitation feature close to the elastic line (white arrow), as previously reported in battery electrodes with oxygen redox
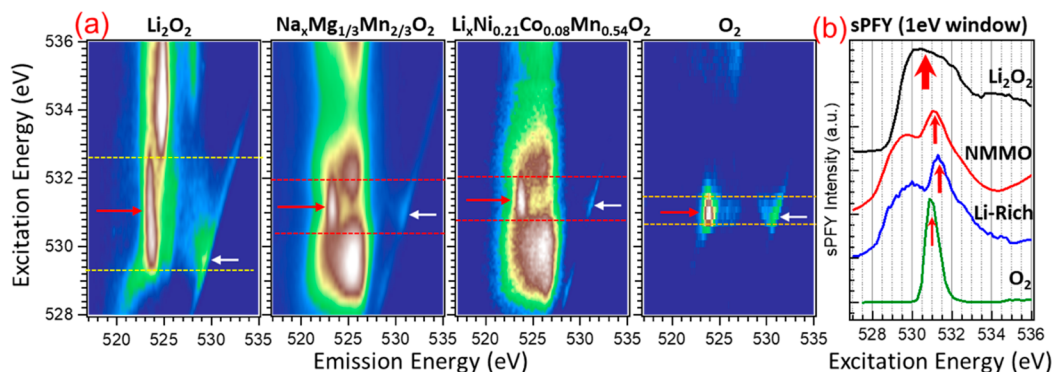

Figure 4. (a) Direct comparison of full mRIXS profile of oxidized oxygen states in four systems: Li_2O_2,[21] charged NMMO ($Na_{2/3}Mg_{1/3}Mn_{2/3}O_2$),[17] charged Li-rich ($Li_{1.17}Ni_{0.21}Co_{0.08}Mn_{0.54}O_2$),[20] and O_2. The full profile reveals that the two groups of characteristic oxidized oxygen features, i.e., the 523.7 eV emission feature (red arrows) and low-energy excitation feature (white arrow), are distinct in their profile along excitation energies. Color scales are adjusted so the horizontal size of the 523.7 eV emission feature remains the same for all the maps. Horizontal dashed lines are plotted at the rising edge of the 523.7 eV feature in (a). The width defined by the lines along excitation energies is proportional to the quantitative analysis of the half peak width of the 531 eV feature in (b). Details of the peak fitting parameters are provided in Figures S1−S3 with peak widths of 0.51, 0.35, and 0.24 eV for NMMO, Li-rich, and O_2, respectively. (b) sPFY spectra of the four systems extracted from mRIXS maps by integrating the intensity within 0.5 eV of the 523.7 eV emission energy. Red arrows indicate the distinct positions of the characteristic features in different systems.

activities.[5,16] However, differences in execution energies of this feature could be easily seen (Figure 4a). While this feature of O_2 is known to be from the vibronic modes of the gas molecule, they are likely of different types of phonon modes in the solid-state Li_2O_2 and battery electrodes.

The direct mRIXS comparison here, especially on the characteristic 523.7 eV emission feature, strongly suggests that the oxidized oxygen state involved in oxygen redox reactions in batteries is not simply through a molecular configuration of either a peroxide type or oxygen gas. Therefore, the ultimate clarifications on the origin of oxygen redox states in TM oxides require future efforts to resolve and calculate the phonon features in RIXS,[29] and particularly, the interpretation of the characteristic 523.7 eV emission feature in oxide systems needs to consider the strong effect from both the TM and oxygen under such a highly oxidized state, which remains a grand challenge but critical for achieving a fundamental understanding of the driving force of oxygen activities in batteries.

In summary, by collecting the full energy range mRIXS of O_2 and CO_2 gas molecules, we show that, although CO_2 is a highly covalent system, the specific feature with ∼523.7 eV emission and low-energy excitation energy in mRIXS does not emerge in CO_2. Therefore, this specific feature is a fingerprint of the intrinsic oxidized oxygen states, not a conventional oxygen state affected by hybridization or covalency. All seven groups of mRIXS features of CO_2 could be reasonably interpreted on the basis of the schematic of the molecular orbitals. We then focus on the direct mRIXS comparison of the oxidized oxygen species between Li_2O_2 (O^-), Li-ion, and Na-ion battery electrodes at charged state with oxidized oxygen (O^{n-}, $0 < n < 2$) and O_2 (O^0) systems. The direct contrast of the mRIXS full profile reveals that, although all these oxidized oxygen species display both the ∼523.7 eV emission feature and an enhanced low-energy excitation feature close to the elastic line, the characteristic feature show different profiles and positions along excitation energies in different systems. The contrast on both the width and positions of the 523.7 eV emission features suggests that the lattice oxygen redox states in batteries are at least not a *pure* molecular configuration of either the peroxide or oxygen gas type. While the fundamental understanding of the oxygen redox mechanism remains a highly debated topic, the direct comparison here provides a critical foundation for understanding the highly oxidized states in a complex transition-metal oxide system. The results indicate and are consistent with the strong association between the transition metal and oxygen in batteries. It is therefore critical to go beyond both a molecular oxygen configuration and the hybridization model to truly understand the oxygen redox activities in oxide electrodes. Considerations of the strong effects from highly oxidized states of both TMs and oxygen should be considered, a challenging topic in both materials and physics. We hope this work clarifies some crucial speculations on the nature of the oxidized oxygen state in oxide electrodes and could raise further attention and efforts toward an ultimate understanding of the oxygen redox mechanism in a broad field of chemistry, material sciences, and fundamental physics.

ASSOCIATED CONTENT

Ⓢ Supporting Information

The Supporting Information is available free of charge at https://pubs.acs.org/doi/10.1021/acs.jpclett.0c00423.

O K-edge sPFY experimental and quantitative analysis fits (PDF)

AUTHOR INFORMATION

Corresponding Authors

Feng Pan − *School of Advanced Materials, Peking University, Shenzhen Graduate School, Shenzhen 518055, People's Republic of China;* ⊙ orcid.org/0000-0002-8216-1339; Email: panfeng@pkusz.edu.cn

Wanli Yang − *Advanced Light Source, Lawrence Berkeley National Laboratory, Berkeley, California 94720, United States;* ⊙ orcid.org/0000-0003-0666-8063; Email: wlyang@lbl.gov

Authors

Zengqing Zhuo − *School of Advanced Materials, Peking University, Shenzhen Graduate School, Shenzhen 518055, People's Republic of China; Advanced Light Source, Lawrence Berkeley National Laboratory, Berkeley, California 94720, United States*

Yi-sheng Liu − *Advanced Light Source, Lawrence Berkeley National Laboratory, Berkeley, California 94720, United States;* ⊙ orcid.org/0000-0002-1085-1947

Jinghua Guo − *Advanced Light Source, Lawrence Berkeley National Laboratory, Berkeley, California 94720, United States;* ⊙ orcid.org/0000-0002-8576-2172

Yi-de Chuang − *Advanced Light Source, Lawrence Berkeley National Laboratory, Berkeley, California 94720, United States;* ⊙ orcid.org/0000-0002-2773-3840

Complete contact information is available at: https://pubs.acs.org/10.1021/acs.jpclett.0c00423

Notes

The authors declare no competing financial interest.

REFERENCES

(1) Grimaud, A.; Hong, W. T.; Shao-Horn, Y.; Tarascon, J. M. Anionic redox processes for electrochemical devices. *Nat. Mater.* **2016**, *15*, 121−126.

(2) Assat, G.; Tarascon, J.-M. Fundamental understanding and practical challenges of anionic redox activity in Li-ion batteries. *Nat. Energy* **2018**, *3*, 373−386.

(3) Saubanere, M.; McCalla, E.; Tarascon, J. M.; Doublet, M. L. The intriguing question of anionic redox in high-energy density cathodes for Li-ion batteries. *Energy Environ. Sci.* **2016**, *9*, 984−991.

(4) Grimaud, A.; Diaz-Morales, O.; Han, B.; Hong, W. T.; Lee, Y.-L.; Giordano, L.; Stoerzinger, K. A.; Koper, M. T. M.; Shao-Horn, Y. Activating lattice oxygen redox reactions in metal oxides to catalyse oxygen evolution. *Nat. Chem.* **2017**, *9*, 457−465.

(5) House, R. A.; Maitra, U.; Pérez-Osorio, M. A.; Lozano, J. G.; Jin, L.; Somerville, J. W.; Duda, L. C.; Nag, A.; Walters, A.; Zhou, K.-J.; Roberts, M. R.; Bruce, P. G. Superstructure control of first-cycle

voltage hysteresis in oxygen-redox cathodes. *Nature* **2020**, *577*, 502−508.

(6) McCalla, E.; Abakumov, A. M.; Saubanere, M.; Foix, D.; Berg, E. J.; Rousse, G.; Doublet, M. L.; Gonbeau, D.; Novak, P.; Van Tendeloo, G.; Dominko, R.; Tarascon, J. M. Visualization of O-O peroxo-like dimers in high-capacity layered oxides for Li-ion batteries. *Science* **2015**, *350*, 1516−1521.

(7) Yang, W. Oxygen release and oxygen redox. *Nat. Energy* **2018**, *3*, 619−620.

(8) Wu, J.; Zhuo, Z.; Rong, X.; Dai, K.; Lebens-Higgins, Z.; Sallis, S.; Pan, F.; Piper, L. F. J.; Liu, G.; Chuang, Y.-d.; Hussain, Z.; Li, Q.; Zeng, R.; Shen, Z.-x.; Yang, W. Dissociate lattice oxygen redox reactions from capacity and voltage drops of battery electrodes. *Sci. Adv.* **2020**, *6*, No. eaaw3871.

(9) Wandt, J.; Freiberg, A. T. S.; Ogrodnik, A.; Gasteiger, H. A. Singlet oxygen evolution from layered transition metal oxide cathode materials and its implications for lithium-ion batteries. *Mater. Today* **2018**, *21*, 825−833.

(10) Qiao, R.; Roychoudhury, S.; Zhuo, Z.; Li, Q.; Lyu, Y.; Kim, J.-H.; Liu, J.; Lee, E.; Polzin, B.; Guo, J.; Yan, S.; Hu, Y.; Li, H.; Prendergast, D.; Yang, W. Deciphering the Oxygen Absorption Pre-Edge: Universal Map of Transition Metal Redox Potentials in Batteries. *ChemRxiv* **2019**.

(11) Lee, G.-H.; Wu, J.; Kim, D.; Cho, K.; Cho, M.; Yang, W.; Kang, Y. M. Reversible Anionic Redox Activities in Conventional LiNi1/3Co1/3Mn1/3O2 Cathodes. *Angew. Chem., Int. Ed.* **2020**, DOI: 10.1002/anie.202001349.

(12) Glans, P.; Gunnelin, K.; Skytt, P.; Guo, J. H.; Wassdahl, N.; Nordgren, J.; Agren, H.; Gelmukhanov, F. K.; Warwick, T.; Rotenberg, E. Resonant x-ray emission spectroscopy of molecular oxygen. *Phys. Rev. Lett.* **1996**, *76*, 2448−2451.

(13) Hennies, F.; Pietzsch, A.; Berglund, M.; Fohlisch, A.; Schmitt, T.; Strocov, V.; Karlsson, H. O.; Andersson, J.; Rubensson, J. E. Resonant inelastic scattering spectra of free molecules with vibrational resolution. *Phys. Rev. Lett.* **2010**, *104*, 193002.

(14) Maganas, D.; Kristiansen, P.; Duda, L.-C.; Knop-Gericke, A.; DeBeer, S.; Schlögl, R.; Neese, F. Combined Experimental and Ab Initio Multireference Configuration Interaction Study of the Resonant Inelastic X-ray Scattering Spectrum of CO2. *J. Phys. Chem. C* **2014**, *118*, 20163−20175.

(15) Cesar, A.; Gel'mukhanov, F.; Luo, Y.; Ågren, H.; Skytt, P.; Glans, P.; Guo, J.; Gunnelin, K.; Nordgren, J. Resonant x-ray scattering beyond the Born−Oppenheimer approximation: Symmetry breaking in the oxygen resonant x-ray emission spectrum of carbon dioxide. *J. Chem. Phys.* **1997**, *106*, 3439−3456.

(16) Wu, J.; Li, Q.; Sallis, S.; Zhuo, Z.; Gent, W. E.; Chueh, W. C.; Yan, S.; Chuang, Y.-d.; Yang, W. Fingerprint Oxygen Redox Reactions in Batteries through High-Efficiency Mapping of Resonant Inelastic X-ray Scattering. *Condensed Matter* **2019**, *4*, 5.

(17) Dai, K.; Wu, J.; Zhuo, Z.; Li, Q.; Sallis, S.; Mao, J.; Ai, G.; Sun, C.; Li, Z.; Gent, W. E.; Chueh, W. C.; Chuang, Y.-d.; Zeng, R.; Shen, Z.-x.; Pan, F.; Yan, S.; Piper, L. F. J.; Hussain, Z.; Liu, G.; Yang, W. High Reversibility of Lattice Oxygen Redox Quantified by Direct Bulk Probes of Both Anionic and Cationic Redox Reactions. *Joule* **2019**, *3*, 518−524.

(18) Yang, W.; Devereaux, T. P. Anionic and cationic redox and interfaces in batteries: Advances from soft X-ray absorption spectroscopy to resonant inelastic scattering. *J. Power Sources* **2018**, *389*, 188−197.

(19) Xu, J.; Sun, M.; Qiao, R.; Renfrew, S. E.; Ma, L.; Wu, T.; Hwang, S.; Nordlund, D.; Su, D.; Amine, K.; Lu, J.; McCloskey, B. D.; Yang, W.; Tong, W. Elucidating anionic oxygen activity in lithium-rich layered oxides. *Nat. Commun.* **2018**, *9*, 947.

(20) Gent, W. E.; Lim, K.; Liang, Y.; Li, Q.; Barnes, T.; Ahn, S.-J.; Stone, K. H.; McIntire, M.; Hong, J.; Song, J. H.; Li, Y.; Mehta, A.; Ermon, S.; Tyliszczak, T.; Kilcoyne, D.; Vine, D.; Park, J.-H.; Doo, S.-K.; Toney, M. F.; Yang, W.; Prendergast, D.; Chueh, W. C. Coupling between oxygen redox and cation migration explains unusual electrochemistry in lithium-rich layered oxides. *Nat. Commun.* **2017**, *8*, 2091.

(21) Zhuo, Z.; Pemmaraju, C. D.; Vinson, J.; Jia, C.; Moritz, B.; Lee, I.; Sallies, S.; Li, Q.; Wu, J.; Dai, K.; Chuang, Y.-d.; Hussain, Z.; Pan, F.; Devereaux, T. P.; Yang, W. Spectroscopic Signature of Oxidized Oxygen States in Peroxides. *J. Phys. Chem. Lett.* **2018**, *9*, 6378−6384.

(22) Qiao, R.; Li, Q.; Zhuo, Z.; Sallis, S.; Fuchs, O.; Blum, M.; Weinhardt, L.; Heske, C.; Pepper, J.; Jones, M.; Brown, A.; Spucces, A.; Chow, K.; Smith, B.; Glans, P.-A.; Chen, Y.; Yan, S.; Pan, F.; Piper, L. F. J.; Denlinger, J.; Guo, J.; Hussain, Z.; Chuang, Y.-D.; Yang, W. High-efficiency in situ resonant inelastic x-ray scattering (iRIXS) endstation at the Advanced Light Source. *Rev. Sci. Instrum.* **2017**, *88*, 033106.

(23) Guo, J. The development of in situ photon-in/photon-out soft X-ray spectroscopy on beamline 7.0.1 at the ALS. *J. Electron Spectrosc. Relat. Phenom.* **2013**, *188*, 71−78.

(24) Chuang, Y.-D.; Shao, Y.-C.; Cruz, A.; Hanzel, K.; Brown, A.; Frano, A.; Qiao, R.; Smith, B.; Domning, E.; Huang, S.-W.; Wray, L. A.; Lee, W.-S.; Shen, Z.-X.; Devereaux, T. P.; Chiou, J.-W.; Pong, W.-F.; Yashchuk, V. V.; Gullikson, E.; Reininger, R.; Yang, W.; Guo, J.; Duarte, R.; Hussain, Z. Modular soft x-ray spectrometer for applications in energy sciences and quantum materials. *Rev. Sci. Instrum.* **2017**, *88*, 013110.

(25) Lebens-Higgins, Z. W.; Vinckeviciute, J.; Wu, J.; Faenza, N. V.; Li, Y.; Sallis, S.; Pereira, N.; Meng, Y. S.; Amatucci, G. G.; Der Ven, A. V.; Yang, W.; Piper, L. F. J. Distinction between Intrinsic and X-ray-Induced Oxidized Oxygen States in Li-Rich 3d Layered Oxides and LiAlO2. *J. Phys. Chem. C* **2019**, *123*, 13201−13207.

(26) Ament, L. J. P.; van Veenendaal, M.; Devereaux, T. P.; Hill, J. P.; van den Brink, J. Resonant inelastic x-ray scattering studies of elementary excitations. *Rev. Mod. Phys.* **2011**, *83*, 705−767.

(27) Housecroft, C. E.; Sharpe, A. G. *Inorganic Chemistry*, Fourth ed.; Person Education Limited, 2012.

(28) Domcke, W.; Cederbaum, L. S. Vibronic Coupling and Symmetry Breaking in Core Electron Ionization. *Chem. Phys.* **1977**, *25*, 189−196.

(29) Devereaux, T. P.; Shvaika, A. M.; Wu, K.; Wohlfeld, K.; Jia, C. J.; Wang, Y.; Moritz, B.; Chaix, L.; Lee, W. S.; Shen, Z. X.; Ghiringhelli, G.; Braicovich, L. Directly Characterizing the Relative Strength and Momentum Dependence of Electron-Phonon Coupling Using Resonant Inelastic X-Ray Scattering. *Phys. Rev. X* **2016**, *6*, 041019.